Research Article | Vol. 27, No. 15 | 22 Jul 2019 | OPTICS EXPRESS 21285
Optics EXPRESS

Form and magnetic birefringence in undulated Permalloy/PET films

MIGUEL A. ARRANZ,[1,*] ELENA H. SÁNCHEZ,[2] ESTHER REBOLLAR,[3] MARTA CASTILLEJO,[3] AND JOSÉ M. COLINO,[2]

[1] *Facultad de Ciencias y Tenologías Quimicas, Universidad de Castilla-La Mancha, Av/ Camilo José Cela 10, 13071 Ciudad Real, Spain*
[2] *Instituto de Nanociencia, Nanotecnología y Materiales Moleculares, Universidad de Castilla-La Mancha, Campus de la Fábrica de Armas, 45071 Toledo, Spain*
[3] *Instituto de Química-Física Rocasolano, Consejo Superior de Investigaciones Científicas Serrano 119, 28006 Madrid, Spain*
[*] *MiguelAngel.Arranz@uclm.es*

Abstract: We report the measurement of form and magnetic birefringence in Permalloy (Ni80Fe20) films grown on rippled Poly(Ethylene Terephthalate), PET, substrates. Prior to Permalloy deposition, Laser Induced Periodic Surface Structures (LIPSS) were generated on the polymeric substrate by a nanosecond laser beam, developing an ordered rippled nanostructure. Due to their high transparency factor, we could investigate the behavior of linear polarized light transmitting at normal incidence on Permalloy/PET sample. The results show the existence of an optical axis parallel to the ripples direction, which yields an strong form birefringence effect arising from the laser patterning. Concerning the Permalloy thin film, the study of its in-plane magnetization was carried out measuring the Voigt magnetooptical effect. The obtained data in our samples reveal the appearance of two different mechanisms to reverse the magnetization, as the external magnetic field is parallel or perpendicular to the ripples direction. Accordingly, the transmitted light shows a magnetic birefringence depending on the relative orientation between the ripple direction, i.e. the optical axis of the LIPSS, and the in-plane magnetization of the Permalloy film.

© 2019 Optical Society of America under the terms of the OSA Open Access Publishing Agreement

1. Introduction

In recent years, the use of pulsed lasers to irradiate different substrates has shown to be a powerful tool to obtain high resolution bidimensional nanostructures. Among these, laser-induced periodic surface structures (LIPSS) have attracted a considerable research interest due to their potential application in high density data storage, microelectronics and microelectromechanical systems [1–3]. For this purpose, various pulse laser durations, ranging from nano to femtosecond regimes, have been used to create ordered nanostructures in different systems, e.g. metals [4], dielectrics or semiconductors [1, 5, 6]. More recently, this research has been also extended to glasses [7, 8] and different polymeric substrates [9–12]. The great resolution of LIPSS arises from the short pulse of high energy, applied on a very localized region of the substrate during laser irradiation. This ultrafast energy deposit rapidly transforms the material with high precision, before the surroundings can be altered. That results in highly localized surface modifications without collateral material damage.

Additionally, the possibility to design and study LIPSS on a transparent matrix opens very interesting research opportunities in optical applications, from both fundamental and applied point of view. After a controlled pulsed laser irradiation, the pristine substrate can evolve from isotropic to anisotropic, concerning the behaviour of transmitted light through the LIPSS. For induced periodic nanostructures with a shape showing a predominant symmetry axis, the polarized light propagates differently depending on the relative direction between its electrical

#362534 https://doi.org/10.1364/OE.27.021285
Journal © 2019 Received 15 Mar 2019; revised 23 May 2019; accepted 27 May 2019; published 16 Jul 2019

Optics EXPRESS

field and the above direction, e.g. two phase velocities and refraction indexes. This optical form effect [13], similar to the birefringence effect in uniaxial crystals, have been reported in LIPSS induced on different glasses [7, 8]. In the case of polymeric substrates, laser irradiation yields corrugated surfaces consisting in a periodic array of ripples, aligning parallel with the incident laser polarization direction [9, 10]. Consequently, this ripple direction breaks the initial shape symmetry of the substrate, being responsible for an expected form birefringence also in these polymeric systems which has not been reported before. The occurrence of this optical effect could turn these polymeric LIPSS into reliable detectors in polarization sensitive flat optics.

In addition, for metallized LIPSS the existence of a well defined anisotropic nanostructure brings about noticeable effects on many physical properties of its capping layer. For instance, the ripple direction yields an strong anisotropy source in both the electrical transport and magnetic properties. As previously reported in rippled cobalt surfaces with ion beam techniques [14, 15], their in-plane magnetization differently reverses as the external magnetic field is applied perpendicular or parallel to the ripples direction. Consequently, a magnetic birefringence effect is observed for transmitting light across that undulated ferromagnetic surface [16]. This could be also applicable to metallized polymeric LIPSS, turning them into sensitive heteroestructures to detect subtle magnetooptical effects.

The use of nanotechnology for generating panostructured patterns in magnetic thin films allows altering the magnetic properties of the material, such as the coercive field, saturation magnetization and magnetic anisotropy. Particularly, magnetic anisotropy is a key ingredient to many applications such as data storage and a variety of magnetic sensors. The generation of patterns, shapes or the introduction of defects in the magnetic thin film, has proven to be an efficient way of altering the basic properties of a material [14, 15, 17–20]. Besides, the control and improvement of magnetic anisotropy will allow new functionalities, as an instance, microwave frequency operation of electronics filters [21]. Special interest lies in magnetic films on plastic substrates as these will allow extra functionalities related to flexible devices. We regard pioneering work by Briones et al. [22] which proved magnetic anisotropy imprint on films grown onto pre-strained PDMS templates. Same polymer materials have been lately used by Li et al. [21] as a substrate for FeCoTa films with static and dynamic anisotropy properties.

In this work, we have first studied the transmitted intensity of polarized light across the rippled PET substrate, focusing on its dependence on the relative orientation between the uniaxial LIPSS and the electrical field direction. The results show the ripple direction to be an effective optical axis, leading to a strong form birefringence in the corrugated polymeric surface. Secondly, we have investigated the capability of that uniaxial LIPSS to also provide a source of anisotropy in the surface magnetization of a capping layer. In this sense, we have measured the Voigt magnetooptical effect of rippled PET substrates coated with different Permalloy thin films.

2. Experimental

2.1. Substrate patterning and Permalloy deposition

Substrates of samples are polymeric poly(ethylene terephthalate) i.e. PET of 125 μm thickness, free-standing films. These foils were nanostructured by scanned irradiation at normal incidence with a linearly polarized laser beam from a Q-switched Nd:YAG laser (Lotis TII LS- 2131M) with pulse duration of 8 ns at a repetition rate of 10 Hz [23]. The fourth harmonic of the fundamental laser radiation at 266 nm was used due to the high absorption coefficient of PET at this wavelength. Formation of LIPSS was achieved at optimum conditions of fluence and number of pulses. Laser fluence was determined by measuring the laser energy in front of the sample and calculating the area of the irradiated spots. Laser fluence typically ranges 8-10 mJ/cm^2. Samples were mounted on a motorized XY translation stage and in order to irradiate larger areas a sample scanning process was used. The scanning speed, and consequently the spatial overlap of successive pulses, was chosen to apply the optimal amount of pulses for LIPSS

Optics EXPRESS

formation, which exceeds 3600. The fluence must reach a minimum value to overcome the glass transition temperature on the surface of the amorphous polymer but are well below the ablation threshold of PET at this wavelength. All polymer foils have been irradiated with a fixed set of beam parameters.

Polycrystalline Ni80Fe20 films were grown at a rate above 1 Å/s by dc sputtering from a 1.5 in. diameter magnetron source on unheated PET foils either with or without surface laser patterning. Film growth required argon gas at pressure $8 \cdot 10^{-3}$ millibars and the substrate was located at the center above the magnetron gun and parallel to the sputter target. In this way the growing film gets rid of any features related with geometrical effects such as columnar defects. Prior to and after the magnetic film deposition a thin 2-3 nm AlO_x layer is sputter grown to prevent oxidation of the magnetic layer. The thickness of as-grown films is determined by ex situ X-ray reflectivity.

2.2. Experimental characterization

A representative surface topography of permalloy films grown on LIPSS foils is shown with the AFM image in the panel of Fig. 1(a). Precise pattern characteristic lengths may slightly vary from sample to sample, irrespective of the thickness of the magnetic layer. As an inset of this Fig. 1(a) appears the histogram of surface ripple amplitudes, i.e. depths, obtained from the same topography image with a number of crest-to-trough excursions taken in a direction locally perpendicular to the ripples. A mean ripple amplitude 42±5 nm roughly corresponds to that of the bare LIPSS polymer (not shown) so, the film surface pattern must have conformally reproduced the film-substrate interface pattern. As we mentioned before this value only slightly varies with the permalloy thickness and is intentionally large for a LIPSS on PET, as compared to previous patterning of the same polymer with different laser dose [24]. The pattern period, i.e. mean spacing, can be extracted from the whole AFM image by means of the 2D Fast Fourier transform which is shown in the inset of panel in Fig. 1(b). Line profiles from the Fourier Transform across the pattern, k_x dependence, and along the pattern, k_y dependence, are curves displayed in the same figure. Up to fourth order peaks show in k_x profiles at a set of k_x values corresponding to a mean period 210 nm. This pattern period is clearly below the irradiating laser wavelength 266 nm; such an effect being expected as the period of LIPSS has been reported to increase with laser fluence and number of pulses until it reaches a plateau for a value of period similar to the irradiating laser wavelength [23]. Either the pattern peaks or the central peak of any profile is just as broad as a result of image size, so the pattern coherence must clearly be larger than the image area. Nonetheless some pattern defects of various types can be observed such "Y-shape" defects (pattern dislocations) and other long-range corrugation probably already present in bare polymer pattern.

As previously commented, the optical characterization were accomplished measuring the transmitted light across the sample. An He-Ne laser beam (633 nm, 1 mW) was focused on the sample surface at normal incidence. The polarization plane of the beam could be adjusted with a Glann-Thompson (GT) polarizer. After, the transmitted light was optically analyzed with (a) a crossed GT polarizer for retardation measurements or (b) a Wollaston prism to investigate both form and magnetic birefringence. In any configuration, the signals were recorded later with fast photodiode detectors and an amplifier circuit. For magnetic measurements, the alternating external field, H, was applied in the sample plane with a 30Hz sweep rate, and its direction could be manually rotated with a 2° precision. Further experimental details are given along each following section.

Optics EXPRESS

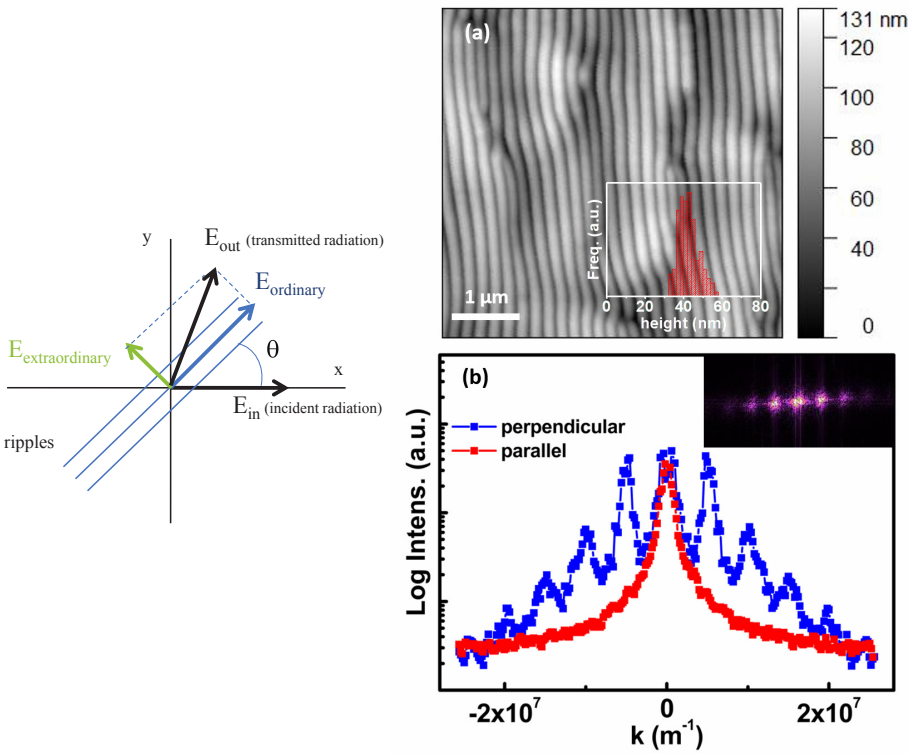

Fig. 1. (Left) Frontal view of the sample along the light path used for measurements in section 3.1. (Right) (a) 5x5 μm^2 AFM topography image of the surface pattern of 20 nm thick permalloy film grown on a PET foil which has previously undergone a LIPSS process. Its inset shows a ripple amplitude histogram from the surface pattern of the topography image. (Right) (b) Line profiles along the main directions (perpendicular=across the pattern, parallel=along the pattern) of a Fourier Transform from the topography image in upper figure. The 2D Fourier Transform image is shown in the inset.

3. Results and discussion

3.1. Form birefringence

To investigate the occurrence of form birefringence in LIPSS patterned onto a PET substrate, we first measured the dependence of transmitted light on the relative orientation between the ripple direction and the polarization plane of incoming beam, angle θ. With the Wollaston prism, the emerging light was decomposed into its orthogonal components, I_x and I_y, the x axis coinciding with the electrical field direction of the incident radiation (drawing in Fig. 1). As an example, the results for a polymeric LIPSS coated with a Permalloy thin film of 10 nm thickness are shown in Fig. 2. Both recorded signals follow the characteristic dependence on $\sin^2\theta$ of an emerging beam whose polarization state is the superposition of two rays oriented at right angle. The ripple direction behaves as an optical axis, splitting the incident light into ordinary and extraordinary rays, with their respective electrical field planes parallel and perpendicular to the ripple direction (see Fig. 1). Around $\theta = 45°$, the polymeric LIPSS fully transforms the polarization state of the incoming beam (maximal I_x), rotating its electrical field 90° in the transmitted light ($I_x \sim 0$). This observed form birefringence arising from the nanostructured PET substrate is much stronger than the inherent birefringence, which exists in some polymeric materials and is due to the initial alignment of the polymeric chains. For a comparison, we have also included in Fig. 2 both I_x

Optics EXPRESS

and I_y measured in a pristine PET foil. It can be seen therein that I_x only decreases around 10% at $\theta = 45°$, showing a partial and much weaker birefringence effect. A further characterization

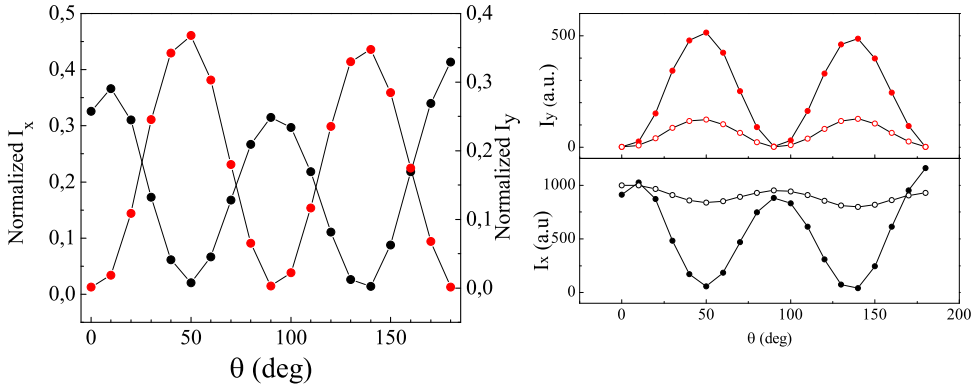

Fig. 2. (Left) Angular dependence of both normalized intensities for the Permalloy(10nm)/PET sample, I_x (black symbols) and I_y (red symbols). (Right) Angular dependence of both intensities for that sample (solid circles) and the flat PET foil (open circles). The I_x curve for the Permalloy(10nm)/PET sample has been vertically shifted for comparison. Lines are guides to the eye.

of the observed form effect in our rippled PET substrates was accomplished by measuring and estimating their retardation factor. For this purpose, the Wollaston prism was substituted by a GT polarizer, crossed with respect to the first polarizer. In this configuration, the intensity of the transmitted light was measured with just one photodetector, and rotating the sample an angular range of $\theta = 0 - 90°$. The angular dependence of the transmitted signal is shown in Fig. 3 for all samples. As seen there, every plot follows the expected $\sin^2 2\theta$ behavior [7], which is also shown in the Eq. (1):

$$T = \frac{\sin^2(2\theta)}{2}(1 - \cos(\delta)) \tag{1}$$

This expression corresponds to the transmitted intensity, T, of a birefringent medium placed

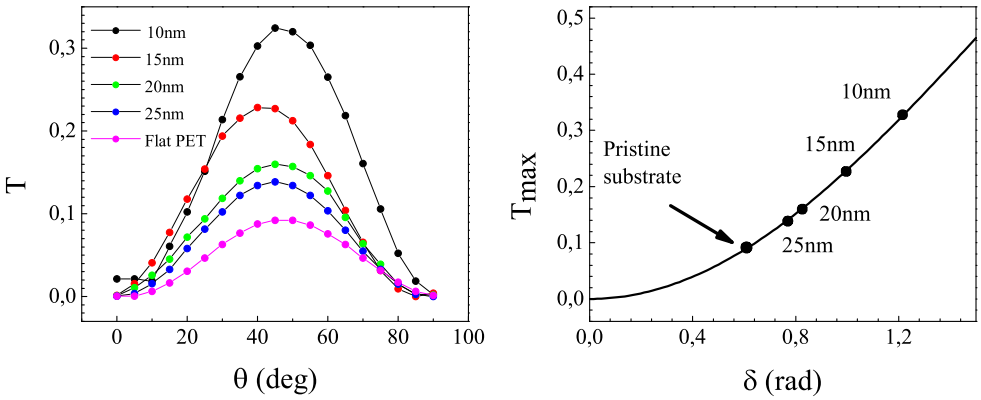

Fig. 3. (left) Angular dependence of T for LIPSS on PET coated with different Permalloy coatings. Lines are guides to the eye. (right) Solid circles are the estimated δ factor from Eq. (1) at $\theta = 45°$ for all measured samples. The solid line corresponds to the representation of that equation. The maximum experimental error for T was $\sim 10^{-3}$

Optics EXPRESS

between two crossed polarizers, where δ is the retardation factor [7, 8]. The estimation of δ value in our LIPSS can be done from the curves displayed in the left panel of Fig. 3, and taking the maximal T measured at $\theta = 45°$. The resulting δ estimations for all samples are shown in the right panel of Fig. 3, beside a plot of the equation (Eq. 1). In all cases, the retardation values are much higher than the one for pristine PET foil, supporting the hypothesis of a strong form birefringence effect in rippled PET substrates. This is particularly clear for the sample with the thinnest Permalloy film (10nm), $\delta \sim 1.21$, where we would approach to the bare rippled PET. A decreasing trend of δ with higher Permalloy thicknesses is also evident from the results, arising from the increasing intensity absorption of the metallic film. In all cases, the retardation values of our LIPSS, originated in the form birefringence effect, stand well above the one for the flat PET foil, and are comparable or higher to reported δ values of LIPSS in glass systems [8].

3.2. Magnetic birefringence

The magnetic characterization of our samples was carried on by investigating the existence of different mechanisms to reverse the in-plane magnetization, M, under an external magnetic field. In bidimensional magnetic systems whose M behaves isotropically, the transmitted light does not undergo any change in its polarization as all in-plane directions are equivalent. On the other hand, for magnetic films showing some in-plane anisotropy direction, different mechanisms rule the magnetization reversal depending on the relative orientation between H and that anisotropy axis. Consequently, the incident beam will traverse the sample with different velocities as its polarization plane is differently affected by M, parallel or perpendicular to the anisotropy axis. That results in a phase shift δ_V and an emerging light elliptically polarized. This magnetic birefringence is the known magnetooptical Voigt effect, $\delta_V \propto n_{\parallel} - n_{\perp}$, where both refraction indexes correspond to polarized radiation with electric vectors parallel or perpendicular to M, respectively [25]. Contrarily to the Kerr rotation for the reflected light, that Voigt effect is quadratic with respect to M and dependent on the off-diagonal terms of the dielectric tensor $\hat{\epsilon}$ of the anisotropic medium magnetically affecting to the transmitted light [26]. The magnetooptical

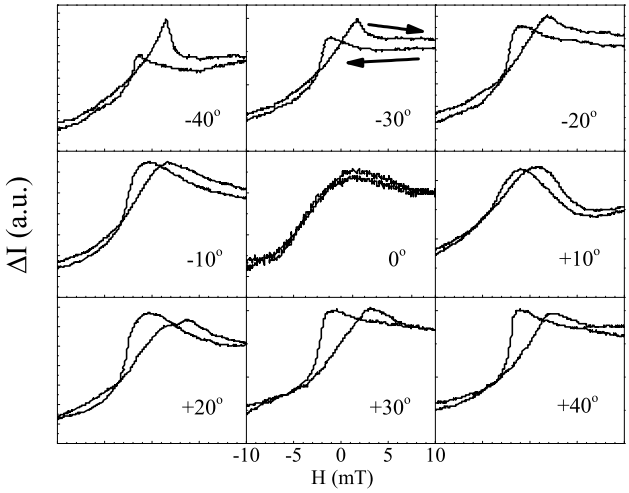

Fig. 4. Raw data of measured differential intensity with H oriented perpendicular to the ripples direction and a range of ±40° (sample with a Permalloy film of 15nm thickness). Arrows indicate the H variation in all panels.

Optics EXPRESS

Voigt effect is extremely smaller than the form birefringence arising from the LIPSS and studied in section 3.1. Some considerations were taken in account to separate both effects. During the whole measurement, the sample was kept with its ripple direction along x axis, and the polarization plane of the incoming radiation oriented $\theta = 45°$ to x axis. In this configuration, both I_x and I_y signals are very similar after emerging from the LIPSS in PET substrate. That enabled us to cancel the form birefringence effect at the differential amplifier circuit, prior to switch the external magnetic field. Thus, the measured signal $\delta_V \propto \Delta I = I_x - I_y$ would only relate to the magnetooptical effect, once H is applied in the sample plane [27]. Experimentally, the magnetic birefringence appears as ΔI peaks when the in-plane magnetization perpendicular to the anisotropy axis, $M_\perp$, reverses coherently over that ripples direction under an external alternating H [28].

For a Permalloy(15nm)/PET sample, the magnetic field dependence of ΔI at different relative orientations between H and the normal direction to the ripples, hereafter Φ, is shown in Fig. 4. As can be seen there, two separated peaks emerge from the background signal at $\Phi = \pm 40°$. As we progressively align H perpendicular to the ripples, their relative distance decreases, reaching zero at $\Phi = 0°$. This behaviour of ΔI in the transmitted radiation has been already observed in rippled Co films showing magnetic birefringence [16, 26]. In this case, the LIPSS written on the PET foil exhibits a well defined ripples direction, periodically extended all over the substrate. After deposition, the magnetic thin film grown on that ripples array reproduces the same spatial pattern, showing a coincident anisotropy axis parallel to the ripples direction. Thus, in this corrugated Permalloy film, two different sources rule the M reversal in such anisotropic system, on one hand, the nucleation and growth of 180° magnetic domains along the ripple direction (easy magnetic axis, EA), on the other hand, the coherent rotation of M perpendicular to the ripple direction (hard magnetic, HA) [15, 29]. The existence of these unlike mechanisms to switch M consequently affects the linear polarized light transmitting across the sample, yielding the occurrence of two intensity peaks centered above the coercive field, H_C, values [28, 30]. As seen in Fig. 4, both intensity peaks merge at $\Phi = 0$ where M is driven parallel to the HA. indicating a complete uniaxial magnetic anisotropy (UMA) in our Permalloy(15nm)/PET sample. That would mean that the polymeric LIPSS are responsible for the existence of two orthogonal magnetic axes, EA and HA, coinciding with the symmetry axes of the ripples array.

Concerning the occurrence of UMA in our Permalloy/PET samples, further insight can be obtained from Fig. 5. Therein, we have focused on measuring ΔI in the vicinity of the HA for two samples with different Permalloy thicknesses, 15 and 25nm. For the thicker sample, the displayed data show two peaks which get close but do not merge completely at $\Phi = 0°$, when H is parallel to the hard magnetic axis. In this case, the anisotropy contribution arising from the ripple array is slightly shadowed by the isotropic in-plane magnetization of the bulk, somewhat more relevant in this thick magnetic film. On the contrary, for the Permalloy(15nm)/PET, the results of the transmitted intensity exhibit an unique intensity peak when H aligns to the HA. According to the frame of those two magnetic contributions, the surface magnetization is fully ruled by the anisotropic rippled LIPSS, leading to the existence of a complete UMA in very thin magnetic layers [16]. As commented above, in the vicinity of the HA, the Voigt effect is basically $\propto M_\perp^2$ and we could outline an expected behaviour of $M_\perp$ under the applied H around HA. In spite of the quadratic dependence of δ_V on H, that simulation could help us to visualize the $M_\perp$ reversal perpendicular to the anisotropy axis ($\Phi = 0$), similarly to vectorial Kerr measurements in nanostructured Co films [15, 29]. These modelized cycles can be seen in the insets of Fig. 5, where the field dependence of $M_\perp$ changes antisimetrycally at $\Delta\Phi = \pm 2°$ over the HA. Finally, we have estimated the coercive field, H_C, of our Permalloy/PET samples from the transmitted intensity data. The relative distance between both peaks is $2H_C$ [28]. The dependence of H_C on the orientation of H with respect to the hard magnetic axis is plotted in Fig. 6, for samples with 15 and 25nm thicknesses. In both cases, an abrupt decrease of H_C clearly appears as H

Optics EXPRESS

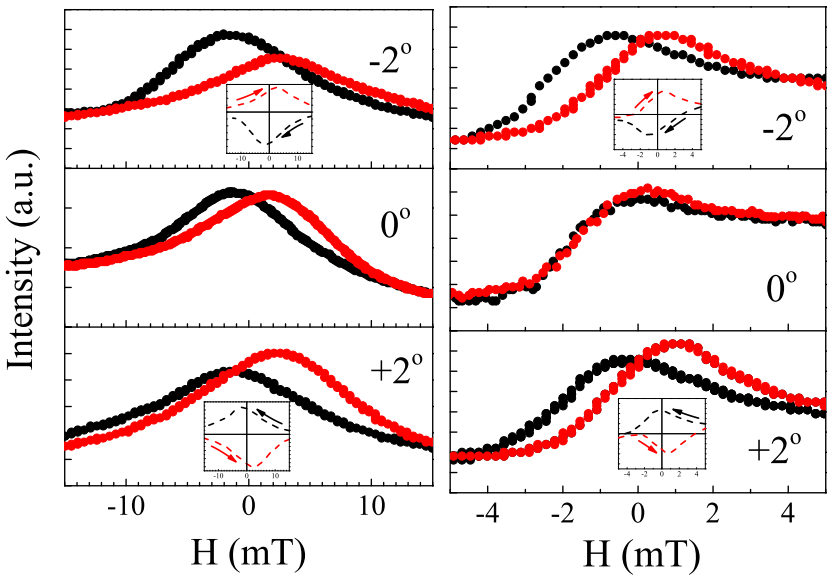

Fig. 5. Measured differential intensity with H oriented near to the perpendicular to the ripples direction (left panel, Permalloy thickness 25nm; right panel Permalloy thickness 15nm). The insets show an estimated field dependence of $M_{\perp}$ near the HA (see the text for details). Symbols and arrows color indicates the H variation: (black) decreasing and (red) increasing.

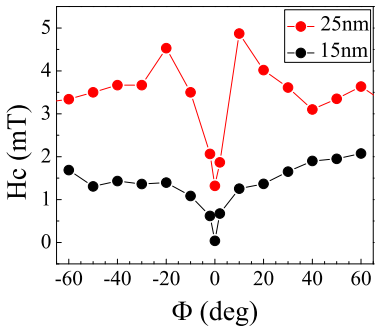

Fig. 6. Angular dependence of the coercive field measured around the normal to ripples direction (HA). The maximum experimental error for H_C was ~ 0.03mT

is aligned perpendicular to the ripples direction. This agrees with the observed merging trend of the intensity peaks. The angular dependence of H_C for the 25 nm thick film shown in Fig. 6 is found first to increase as the field direction approaches the hard axis and then decrease precisely at the hard axis. This behavior is in agreement with a so-called two-phase model of magnetization reversal, whereby the film (area probed with transmitting laser) consists of two different types of domains with either rotational coercivity or domain wall pinning type of coercivity [31]. Recently, Li and coworkers [21] have reported a similar behavior in FeCoTa films grown on wrinkled surface and good quantitative agreement with two-phase model. Further analysis of magnetization reversal mechanisms will be the subject of a forthcoming article. From the quantitative point of view, H_C curve does not vanish at $\Phi = 0$, indicating a partial UMA in the thicker Permalloy film. Contrarily, the H_C data for the Permalloy(15nm)/PET drastically change from an approximate constant value to zero, as the in-plane magnetization reversal is

Optics EXPRESS

accomplished along the EA or the HA. This would point on the polymeric LIPSS to be able to induce UMA in the Permalloy coating, and therefore, magnetic birefringence.

4. Conclusion

In summary, we have successfully fabricated bidimensional heterostructures consisting in LIPSS on a polymeric PET substrate coated with a Permalloy thin film. The LIPSS developed a well defined ripple structure with a periodicity comparable to the incident laser radiation. The study of the transmitted polarized light across these heterostructures revealed an strong form birefringence arising from that rippled surface. We have shown the ripple direction to behave as an optical axis, splitting the incoming radiation in ordinary and extraordinary rays. For LIPSS with a thin magnetic layer, the estimated retardation factor (~ 1.2) between those rays was higher than reported values in other birefringent LIPSS. Additionally, we have studied the magnetooptical Voigt effect in the in-plane magnetization of our Permalloy/PET systems. The obtained results show the existence of magnetic birefringence, also originated from the polymeric LIPSS. Their ripples direction introduces as well a magnetic anisotropy axis in the surface magnetization of the Permalloy film. That leads to the appearance of dissimilar mechanisms for the magnetization reversal, parallel or perpendicular to that ripples direction. Our results evidence the occurrence of a complete uniaxial magnetic anisotropy in LIPSS coated with a Permalloy thin film. All the above seems to put metallized polymeric LIPSS forward promising heterostructures to be applied in optical and magnetooptical devices.

Funding

Spanish Ministry of Economy and Competitiveness, MINECO, (MAT2015-65295-R and CTQ2016-75880-P).

Acknowledgements

E.R. also thanks MINECO for a Ramón y Cajal contract (RYC-2011-08069).

References

1. B. Tan and K. Venkatakrishnan, "A femtosecond laser-induced periodical surface structure on crystalline silicon," J. Micromech. Microeng. **16**, 1–6 (2006).
2. X. Y. Chen, Y. F. Lu, B. J. Cho, Y. P. Zeng, J. N. Zeng, and Y. H. Wu, "Pattern-induced ripple structures at silicon-oxide/silicon interface by excimer laser irradiation." Appl. Phys. Lett. **81**, 1344–1347 (2002).
3. R. L. Harzic, H. Schuck, D. Sauer, T. Anhut, I. Riemann, and K. König, "Sub-100 nm nanostructuring of silicon by ultrashort laser pulses." Opt. Express **13**, 6651–6655 (2005).
4. T. T. D. Huynh, A. Petit, and N. Semmar, "Picosecond laser induced periodic surface structure on copper thin films," Appl. Surf. Sci. **302**, 109–113 (2014).
5. A. Cerkauskaite, R. Drevinskas, A. Solodar, I. Abdulhalim, and P. G. Kazansky, "Form-birefringence in ITO thin films engineered by ultrafast laser nanostructuring," ACS Photonics **4**, 2944–2951 (2017).
6. A. Cerkauskaite, R. Drevinskas, A. O. Rybaltovskii, and P. G. Kazansky, "Ultrafast laser-induced birefringence in various porosity silica glasses: from fused silica to aerogel," Opt. Express **25**, 8011–8021 (2017).
7. P. Yang, G. R. Burns, J. Guo, T. S. Luk, and G. A. Vawter, "Femtosecond laser-pulse-induced birefringence in optically isotropic glass," J. Appl. Phys. **95**, 5280–5283 (2004).
8. S. Richter, C. Miese, S. Döring, F. Zimmermann, M. J. Withford, A. Tünnermann, and S. Nolte, "Laser induced nanogratings beyond fused silica-periodic nanostructures in borosilicate glasses and ULE^{tm}," Opt. Mat. Express **3**, 1161–1166 (2013).
9. M. Castillejo, T. A. Ezquerra, M. O. Margarita Martín and, S. Péreza, and E. Rebollar, "Laser nanostructuring of polymers: ripples and applications," AIP Conf. Proc. **1464**, 372–380 (2012).
10. P. Slepička, O. Neděla, J. Siegel, R. Krajcar, Z. Kolská, and V. Švorčík, "Ripple polystyrene nano-pattern induced by KrF laser," eXPRESS Polym. Lett. **8**, 459–466 (2014).
11. S. Bagheri-Khoulenjani and H. Mirzadeh, "Polystyrene surface modification using excimer laser and radiofrequency plasma: Blood compatibility evaluations." Prog. Biomater. **1**, 1–8 (2012).
12. H. Y. Zheng, T. T. Tan, and W. Zhou, "Studies of KrF laser induced long periodic structures on polyimide evaluations." Opt. Lasers Eng. **47**, 180–185 (2009).

Optics EXPRESS

13. E. Bricchi, B. G. Klappauf, and P. G. Kazansky, "Form birefringence and negative index change created by femtosecond direct writing in transparent materials," Opt. Lett. **29**, 119–121 (2004).
14. R. Moroni, D. Sekiba, F. B. de Mongeot, G. Gonella, C. Boragno, L. Mattera, and U. Valbusa, "Uniaxial magnetic anisotropy in nanostructured Co/Cu(001): from surface ripples to nanowires," Phys. Rev. Lett. **91**, 7027–7030 (2003).
15. M. A. Arranz, J. M. Colino, and F. J. Palomares, "On the limits of uniaxial magnetic anisotropy tuning by a ripple surface pattern," J. Appl. Phys. **115**, 3906–3914 (2014).
16. M. A. Arranz and J. M. Colino, "Angular tuning of the magnetic birefringence in rippled cobalt films," Appl. Phys. Lett. **106**, 3102–3105 (2015).
17. M. Ali, "Growth and study of magnetostrictive FeSiBC thin films for device applications," Ph.D. thesis, University of Sheffield (1999).
18. S. S. P. Parkin, M. Hayashi, and L. Thomas, "Domain-wall racetrack memory," Science **320**, 190–194 (2008).
19. G. Francis, "Data storage-trends and directions," Tech. rep., Oracle Corporation, web.stanford.edu (2011). PASIG-January2012.
20. A. Fernández-Pacheco, R. Streubel, O. Fruchart, P. F. R. Hertel and, and R. P. Cowburn, "Three-dimensional nanomagnetism," Nat. Commun. **8**, 15756–15769 (2017).
21. J. Li, Q. Zhang, S. Zhang, J. Wei, J. Wang, M. Pan, Y. Xie, H. Yang, Z. Zhou, S. Xie, B. Wang, and R.-W. Li, "Magnetic anisotropy and high-frequency property of flexible FeCoTa films obliquely deposited on a wrinkled topography," Nat. Sci. Reports **7**, 2837–2843 (2017).
22. J. Briones, P. Toro, A. Encinas, L. Caballero, J. C. Denardin, F. Melo, E. Cerda, S. Robert, D. Lacour, and F. Montaigne, "Large area patterned magnetic films by depositing cobalt layers on nano-wrinkled polydimethylsiloxane templates," Appl. Phys. Lett. **103**, 2404–2407 (2013).
23. E. Rebollar, M. Castillejo, and T. Ezquerra, "Laser induced periodic surface structures on polymer films: from fundamentals to applications," Eur. Polym. J. **73**, 162–174 (2015).
24. E. Rebollar, S. Pérez, J. J. Hernández, I. Martín-Fabiani, D. R. Rueda, T. A. Ezquerra, and M. Castillejo, "Assessment and formation mechanism of laser-induced periodic surface structures on polymer spin-coated films in real and reciprocal." Langmuir **27**, 5596–5606 (2011).
25. A. Sokolov, *Optical properties of metals* (Blackie, London, 1967), 1st ed.
26. M. A. Arranz and J. M. Colino, "Magnetooptical Voigt effect in rippled polycrystalline Co films," J. Phys. D: Appl. Phys. **49**, 5306–5313 (2016).
27. E. D. Palik, "The use of polarized infrared radiation in magneto-optical studies of semiconductors," Appl. Opt. **2**, 527–539 (1963).
28. R. Carey, B. W. J. Thomas, I. V. F. Viney, and G. H. Weaver, "Magnetic birefringence in thin ferromagnetic films," J. Phys. D **1**, 1679–1684 (1968).
29. J. M. Colino, M. A. Arranz, A. J. Barbero, A. Bollero, and J. Camarero, "Surface magnetization and the role of pattern defects in various types of ripple patterned films," J. Phys. D: Appl. Phys. **49**, 5002–5011 (2016).
30. R. Carey and B. W. J. Thomas, "An improved method of measuring the Voigt effect in thin magnetic films," J. Phys. E: Sci. Instr. **4**, 545–547 (1971).
31. N. P. Suponev, R. M. Grechishkin, M. B. Lyakhova, and Y. E. Pushkar, "Angular dependence of coercive field in (Sm,Zr) (Co,Cu,Fe)z alloys," J. Magn. Magn. Mater. **157/158**, 376–377 (1996).

83.53.138.107 (to 2020-04-02 03:57:54)